

## Pulsed current activated synthesis and consolidation of a nanostructured Cr<sub>2</sub>Zr-ZrO<sub>2</sub> composite and its mechanical properties

In-Jin Shon<sup>a,\*</sup>, Jin-Kook Yoon<sup>b</sup> and Kyung-Tae Hong<sup>b</sup>

<sup>a</sup>Division of Advanced Materials Engineering, the Research Center of Hydrogen Fuel Cell, Chonbuk National University, 664-14 Deokjin-dong 1-ga, Deokjin-gu, Jeonju, Jeonbuk 561-756, Korea

<sup>b</sup>Materials Architecturing Research Center, Korea Institute of Science and Technology, P.O. Box 131, Cheongryang, Seoul 130-650, Korea

ZrO<sub>2</sub> has been used for hip and knee joint replacements because of the excellent combination of biocompatibility, low density and corrosion resistance. However, coarse-grained ZrO<sub>2</sub> has low wear, abrasion resistance and fracture toughness. One of the methods to improve mechanical properties is generally to refine the grain size. As nanomaterials possess high strength, high hardness, excellent ductility and toughness, undoubtedly, more attention has been paid for the application of nanomaterials Cr<sub>2</sub>Zr-1.5ZrO<sub>2</sub> composite was simultaneously synthesized and consolidated by pulsed current activated heating within two min from mechanically milled powders. Highly dense nanostructured Cr<sub>2</sub>Zr-1.5ZrO<sub>2</sub> composite with a relative density of up to 98.5% was produced under application of an 80 MPa pressure with the pulsed current. The mechanical properties and microstructure of the Cr<sub>2</sub>Zr-1.5ZrO<sub>2</sub> composite was investigated using Vickers hardness measurement, X-ray diffraction analysis and Scanning electron microscope observation.

**Key words:** Microstructure, Composites, Nanostructures, Mechanical properties, Chemical synthesis.

### Introduction

ZrO<sub>2</sub>, in its pure form, exhibits three well-defined polymorphs. At room temperature, ZrO<sub>2</sub> has a monoclinic crystal structure. The monoclinic structures changes to a tetragonal form above 1170 °C and to a cubic fluorite structure above 2370 °C. The monoclinic/tetragonal transformation in ZrO<sub>2</sub> is thermodynamically reversible but associated with a large volume change (3 to 5%) (contraction on heating and expansion on cooling). The cubic phase exists up to the melting point of 2680 °C. However, the addition of certain aliovalent oxides can stabilize the cubic fluorite structure of ZrO<sub>2</sub> from room temperature to its melting point. ZrO<sub>2</sub> has been used for hip and knee joint replacements because of the excellent combination of biocompatibility, low density and corrosion resistance [1]. However, coarse-grained ZrO<sub>2</sub> has low wear and abrasion resistance because of its low hardness.

Nanocrystalline materials have received much attention as advanced engineering materials with improved physical and mechanical properties. As nanomaterials possess high strength, high hardness, excellent ductility and toughness, undoubtedly, more attention has been paid for the application of nanomaterials [2, 3]. In recent days, nanocrystalline powders have been developed by the thermochemical and thermomechanical process named

the spray conversion process (SCP), co-precipitation and high energy milling [4-7]. High energy ball milling during the methods reduced the sintering temperature due to the increased reactivity, internal and surface energies, and surface area of the milled powder, which contribute to its so-called mechanical activation [8-10]. However, the grain size in sintered materials becomes much larger than that in pre-sintered powders due to the rapid grain growth during a conventional sintering process. So, controlling grain growth during sintering is one of the keys to the commercial success of nanostructured materials. Unconventional sintering techniques, including high-pressure densification, magnetic pulse compaction and shock densification, have been proposed to overcome the problem of grain growth [11-13]. However, these methods have failed to provide fast, reproducible techniques that yield large quantities of high density samples with nanostructured grains.

The pulsed current activated sintering (PCAS) method has recently emerged as an effective technique for sintering and consolidating high temperature materials [14-16]. PCAS is similar to traditional hot-pressing, but the sample is heated by a pulsed electric current that flows through the sample and a die. This process increases the heating rate (up to 2000 K minute<sup>-1</sup>) to a degree much higher than that of traditional hot-press sintering.

In this study, we investigated simultaneous synthesis and sintering of Cr<sub>2</sub>Zr-1.5 ZrO<sub>2</sub> composites by the PCAS method. The goal of this research is to produce nanopowder and highly dense nanostructured Cr<sub>2</sub>Zr-

\*Corresponding author:  
Tel : +82-63-270-2381  
Fax: +82-63-270-2386  
E-mail: ijshon@jbnu.ac.kr

1.5ZrO<sub>2</sub> material. In addition, we also evaluate the mechanical properties and microstructure of the composites.

### Experimental Procedure

Pure Cr<sub>2</sub>O<sub>3</sub> (99%, -325 mesh, Aesar Inc.) and pure Zr (99 %, -325 mesh, Sejong Inc.) powders were used as raw materials. Cr<sub>2</sub>O<sub>3</sub> and 2.5 Zr powders were mixed in a high-energy ball mill. A Pulverisette-5 planetary mill was used at 250 rpm for 10 h. Tungsten carbide balls (10 mm in diameter) were used for milling in a sealed cylindrical stainless steel vial under an argon atmosphere. The weight ratio of ball-to-powder was 20 : 1.

The milled powders were placed in a graphite die (outside diameter, 35 mm; inside diameter, 10 mm; height, 40 mm) and then introduced into the pulsed current activated sintering (PCAS) system made by Eltek Co. in the Republic of Korea. A schematic diagram of this system is shown in Ref. [14]. The PCAS apparatus includes a 30-kW power supply and a uniaxial press with a maximum load of 50 kN. The system was first evacuated and a uniaxial pressure of 80 MPa was applied. A pulsed current (on time ; 20 μs, off time; 10 μs) was then activated and maintained until the densification rate became negligible, as indicated by the observed shrinkage of the sample. Sample shrinkage was measured in real time by a linear gauge measuring the vertical displacement. Temperature was measured by a pyrometer focused on the surface of the graphite die. The heating rates were approximately 1000 K minute<sup>-1</sup> during the process. At the end of the process, the pulsed current was turned off and the sample was allowed to cool to room temperature. The process was carried out under a vacuum of 10 Pa.

The relative densities of the sintered samples were measured by Archimedes principle. Microstructural information was obtained from the polished surfaces. Compositional and microstructural analyses of the samples were carried out through X-ray diffraction (XRD) analysis, and field-emission scanning electron microscopy (FE-SEM) observation with energy dispersive X-ray spectrometry (EDS). Vickers hardness was measured by performing indentations at a load of 10 kg<sub>f</sub> with a dwell time of 15 s. The grain sizes were calculated by Suryanarayana and Norton's formula [17].

### Results and Discussion

Fig. 1 shows FE-SEM images of raw powders. chromium oxide and Zirconium have irregular shape. X-ray diffraction patterns of raw powders are shown in Fig. 2. Fig. 3 shows an FE-SEM image (a) and the EDS analysis (b) of powders milled for 10 h by the high-energy ball milling method. The powders are very fine and have some agglomeration. The milling process

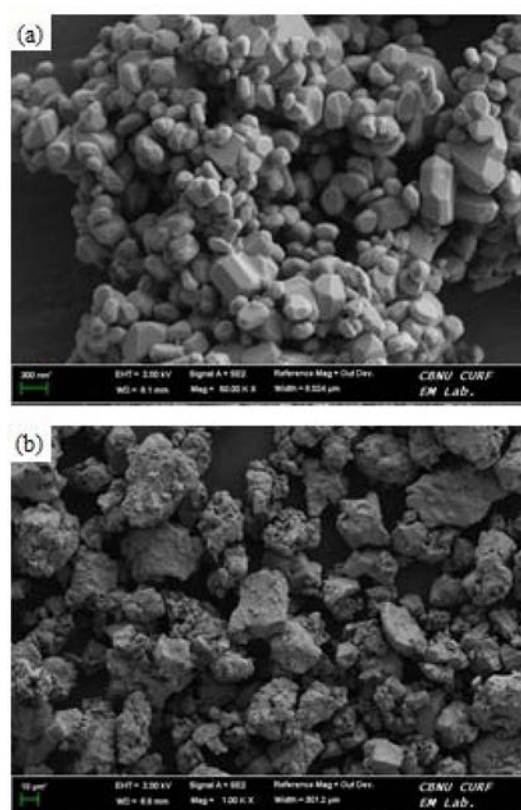


Fig. 1. FE-SEM images of raw powders: (a) Cr<sub>2</sub>O<sub>3</sub> and (b) Zr.

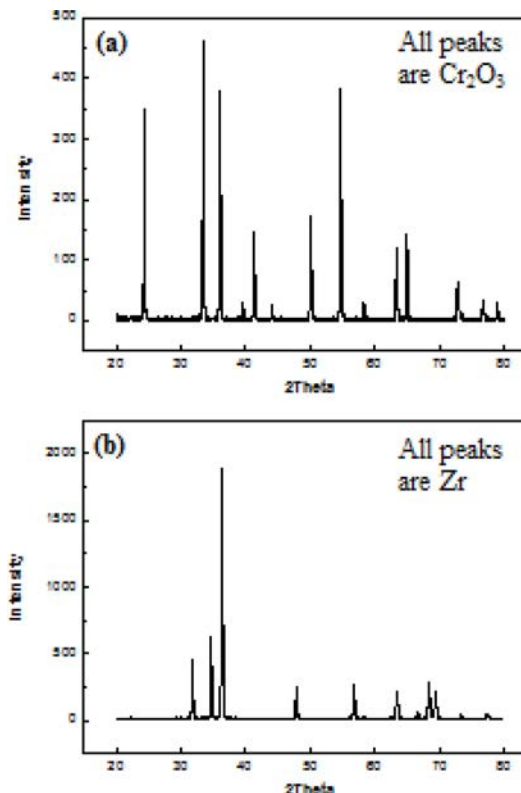


Fig. 2. XRD patterns of raw powders: (a) Cr<sub>2</sub>O<sub>3</sub> and (b) Zr.

is known to introduce impurities from the ball and/or container. However, in this study, peaks other than Zr,

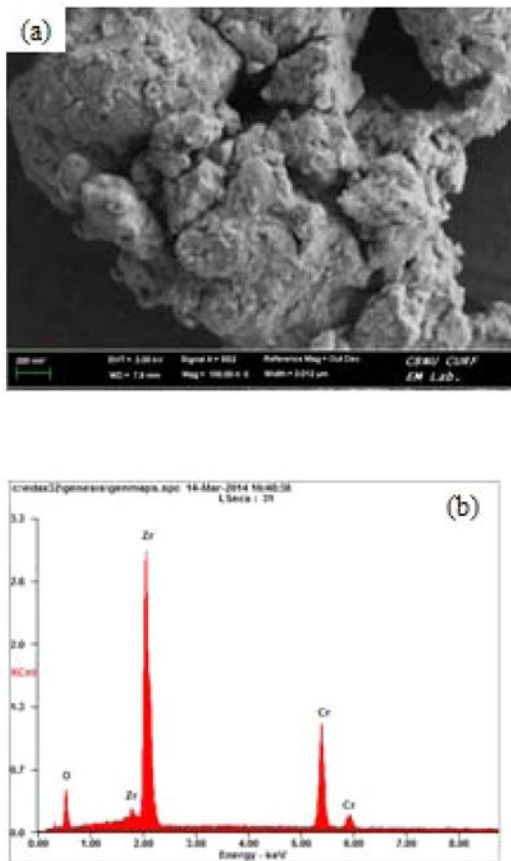


Fig. 3. (a) FE-SEM image and (b) EDS analysis of the powders milled for 10 h.

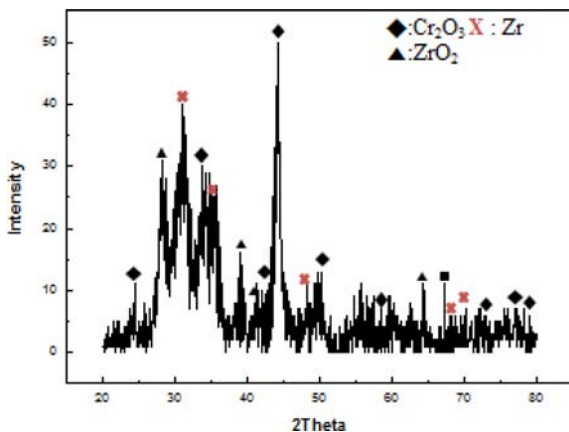


Fig. 4. XRD pattern of  $\text{Cr}_2\text{O}_3 + \text{Zr}$  powders milled for 10 h.

Cr and O were not identified. X-ray diffraction pattern of high-energy ball milled powders is shown in Fig. 4. Peaks of reactants ( $\text{Cr}_2\text{O}_3$  and Zr) were mainly identified after milling. This indicates that synthesis did not occur during the high-energy ball milling method. However, the full width at half-maximum (FWHM) of the diffraction peak in Fig. 4 is more broad than that in Fig. 2(a) and (b) due to the refinement of powders and strains.

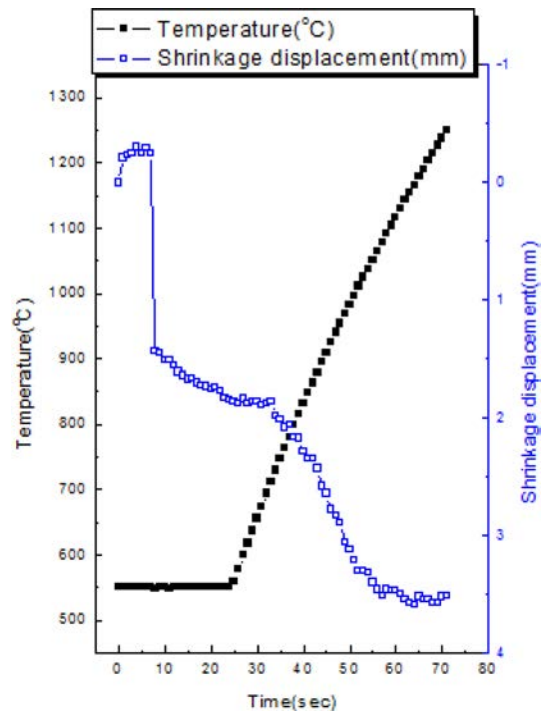


Fig. 5. Variations of temperature and shrinkage displacement with heating time during the pulsed current activated heating of milled powders.

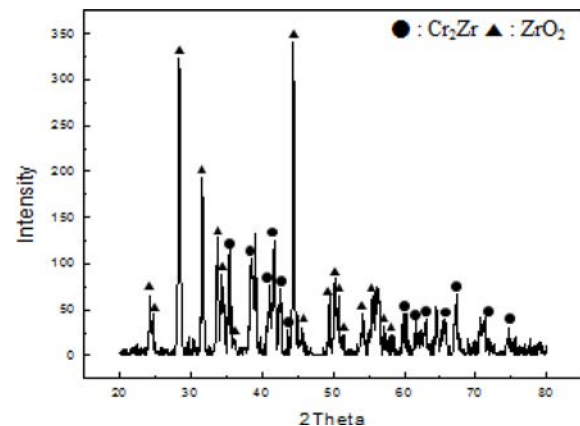
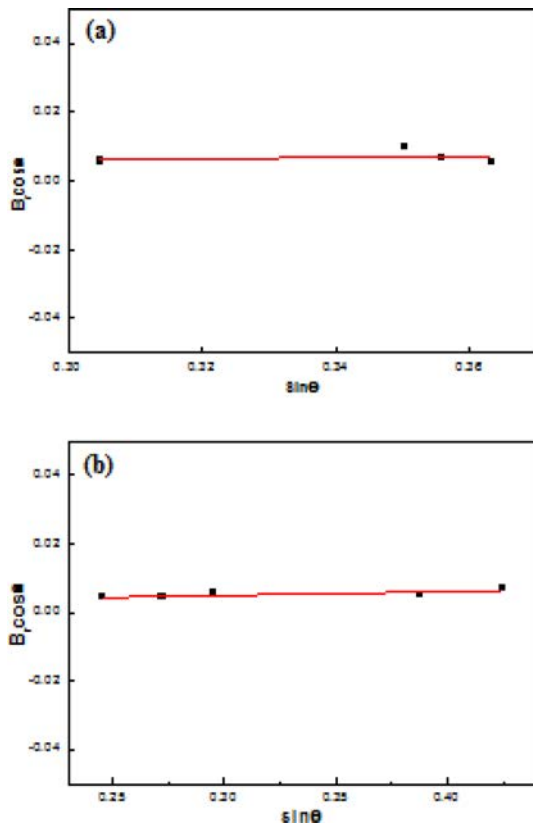
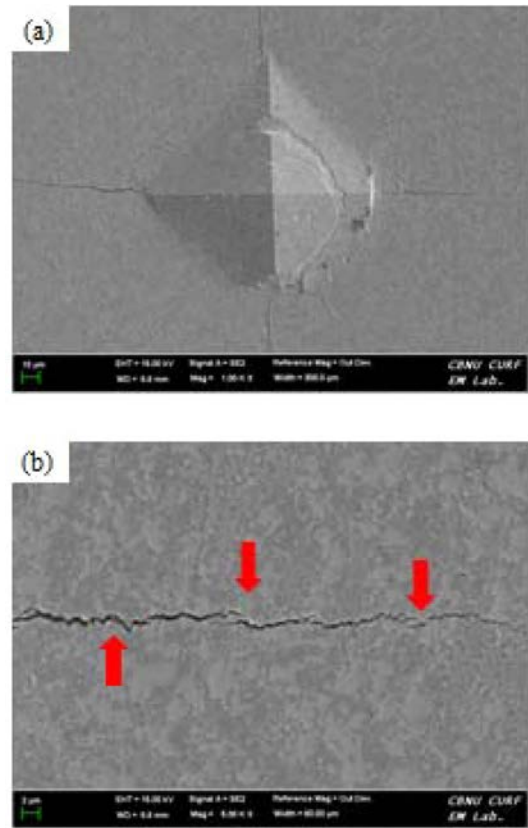


Fig. 6. XRD pattern of the  $\text{Cr}_2\text{Zr}-1.5\text{ZrO}_2$  composite sintered by PCAS.

Fig. 5 shows the variations in shrinkage displacement and temperature of the surface of the graphite die with heating time during the processing of milled powders. The application of the pulsed current resulted in shrinkage due to consolidation. As the pulsed current was applied, thermal expansion shows up to a heating time of 5 s and then the shrinkage displacement abruptly increased. And the shrinkage displacement gradually increased with temperature up to about 1250 °C. X-ray diffraction results for a specimen heated to 1250 °C is shown in Fig. 6. The figure exhibits only peaks pertaining to the  $\text{ZrO}_2$  and  $\text{Cr}_2\text{Zr}$ . From the above results



**Fig. 7.** Plot of  $Br \cos\theta$  versus  $\sin\theta$  for (a) Cr<sub>2</sub>Zr and (b) ZrO<sub>2</sub> in composite sintered by PCAS.



**Fig. 9.** (a) Vickers hardness indentation and (b) crack propagation in a Cr<sub>2</sub>Zr-1.5ZrO<sub>2</sub> composite sintered by PCAS.

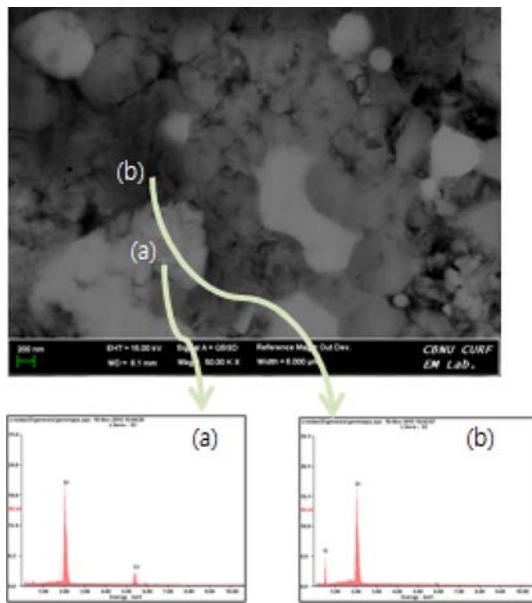
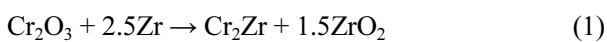


**Fig. 8.** FE-SEM image and EDS of the Cr<sub>2</sub>Zr-1.5ZrO<sub>2</sub> composite sintered by PCAS.

the interaction between Cr<sub>2</sub>O<sub>3</sub> and 2.5 Zr, via



is thermodynamically feasible.

The abrupt increase in the shrinkage displacement at

the ignition temperature in Fig. 5 is due to the increase in density as a result of the molar volume change associated with the formation of Cr<sub>2</sub>Zr + 1.5ZrO<sub>2</sub> from Cr<sub>2</sub>O<sub>3</sub> + 2.5Zr reactants and the consolidation of the product. Fig. 7 shows plots of  $Br \cos\theta$  versus  $\sin\theta$  to calculate average grain size of Cr<sub>2</sub>Zr and ZrO<sub>2</sub> using the formula of Suryanarayana and Grant Norton [17]. The grain sizes were about 57 and 86 nm, respectively. Back scattered electron image and EDS of surface of sample heated to 1250 °C under a pressure of 80 Mpa were shown in Fig. 8. In the FE-SEM image, the bright phase a) is Cr<sub>2</sub>Zr and the grey phase b) is ZrO<sub>2</sub>, due to mass contrast. The corresponding relative density is about 98.5%. It is apparent that the Cr<sub>2</sub>Zr and ZrO<sub>2</sub> grains consist of nanocrystallites, suggesting the absence of grain growth during sintering. This retention of the fine grain structure can be attributed to the high heating rate and the relatively short exposure to high temperature.

After milling, the milled powder was consolidated by PCAS at 1250 °C within two min. These powders were sintered under the application of high pressure (80 MPa) which had a significant effect on the total driving force [18]. Secondly, the role of the current in sintering has been the focus of several attempts aimed at providing an explanation for the observed enhancement of sintering. The role played by the current has been interpreted in

various ways, the effect being explained in terms of the fast heating rate due to Joule heating, the presence of plasma in pores separating powder particles, the enhancement of wettability under the electric field and the intrinsic contribution of the current to fast mass transport [19-21].

Vickers hardness measurements were made on polished sections of the  $\text{Cr}_2\text{Zr-1.5ZrO}_2$  composite using a 10 kg<sub>f</sub> load and a 15s dwell time. The calculated

hardness value of an  $\text{Cr}_2\text{Zr-1.5ZrO}_2$  composite sintered at 1250 °C from high-energy ball milled powders was 905 kg/mm<sup>2</sup>. This value is an average of five measurements. Indentations with large enough loads produced median cracks around the indentation. The lengths of these cracks permit estimation of the fracture toughness of the materials by means of the Niihara's expression [22]. As in the case of hardness values, the toughness values were derived from the average of five measurements. The toughness value of the composite obtained from high-energy ball milled powders is 5.3 MPa·m<sup>1/2</sup>. The hardness and fracture toughness of monolithic  $\text{ZrO}_2$  have been reported as respectively 730 kg/mm<sup>2</sup> and 3.8 MPa·m<sup>1/2</sup> [23]. The mechanical properties (hardness and fracture toughness) of a  $\text{Cr}_2\text{Zr-1.5ZrO}_2$  composite of this study is better than those of a monolithic  $\text{ZrO}_2$  [23] due to the grain refinement. Fig. 9(a) shows the Vickers indentation in a  $\text{Cr}_2\text{Zr-1.5ZrO}_2$  composite sintered by pulsed current activated heating. One to three additional cracks were observed to propagate from the indentation corner and cracks propagated in a deflective (↑) and branching (↓) manner, as shown in

Fig. 9(b). The enhanced fracture toughness of the  $\text{Cr}_2\text{Zr-1.5ZrO}_2$  composite compared to that of pure  $\text{ZrO}_2$  which has been reported as 3.8 MPa·m<sup>1/2</sup> [23] is believed that  $\text{Cr}_2\text{Zr}$  and  $\text{ZrO}_2$  with nanostructure phases in the composite may deter the propagation of cracks.

## Conclusions

Using the pulsed current activated heating method, simultaneous synthesis and densification of a nanostructured  $\text{Cr}_2\text{Zr-1.5ZrO}_2$  composite was accomplished within a duration of two min. The relative density of the composite was 98.5% for the applied pressure of 80 MPa with the pulsed current. The average grain sizes of  $\text{Cr}_2\text{Zr}$  and  $\text{ZrO}_2$  prepared by the pulsed current sintering were about 57 and 86 nm, respectively. The average hardness and fracture toughness values obtained were 905 kg/mm<sup>2</sup> and 5.3 MPa·m<sup>1/2</sup>, respectively. The hardness and fracture toughness of a  $\text{Cr}_2\text{Zr-1.5ZrO}_2$  composite of this study is better than those of a monolithic  $\text{ZrO}_2$  due to the grain refinement and deterring crack propagation by  $\text{Cr}_2\text{Zr}$  and  $\text{ZrO}_2$ .

## Acknowledgments

This work was supported by the KIST Institutional Program (Project No. 2E 26980-17-026) and this research was supported by Basic Science Research Program through the National Research Foundation of Korea (NRF) funded by the Ministry of Education (2015R1D1A1A01056600).

## References

1. B.S. Bal, J.P. Garino, M.D. Ries, M.N. Rahaman,, Semi. Arthroplasty 17 (2006) 94-101.
2. K. Niihara, A. Nikahira, Advanced structural inorganic composite, Elsevier Scientific Publishing Co., Trieste, Italy (1990).
3. Bong-Won Kwak, Seung-Jin Oh, Byung-Su Kim, Jin-Kook Yoon, and In-Jin Shon, Korean J. Met.Mater. 54 (2016) 180-186.
4. Z. Fang, J.W. Eason, Int. J. Refract. Met. Hard Mater. 13 (1995) 297-303.
5. A.I.Y. Tok, L.H. Luo, F.Y.C. Boey, Mater. Sci. Eng. A. 383 (2004) 229-234.
6. Bong-Won Kwak, Seok-Jae Lee and In-Jin Shon, Korean J. Met.Mater. 54 (2016) 409-414.
7. Bo-Ram Kang and In-Jin Shon, Korean J. Met. Mater. 53 (2015) 320-325.
8. F. Charlot, E. Gaffet, B. Zeghamati, F. Bernard, J.C. Liepce, Mater. Sci. Eng. A 262 (1999) 279-278.
9. In-Jin Shon, Hyoung-Gon Jo, Byung-Su Kim, Jin-Kook Yoon, and Kyung-Tae Hong, Korean J. Met. Mater. 53 (2015) 474-479.
10. M.K. Beyer, H. Clausen-Schaumann, Chem. Rev. 105 (2005) 2921-2948.
11. SC Liao, WE Mayo, KD Pae, Acta Mater 45, (1997) 4027-4032.
12. ZQ Jin, C Rockett, JP Liu, K Hokamoto, NN Thadhani, Mater Sci Forum 465-466, (2004) 93-96.
13. V Ivanov, S Paranin, V Khrustov, A Medvedev, A Shtolts, Key Eng Mater 206-213, (2002) 377-381.
14. So-Mang Kwon, Na-Ra Park, Jae-Won Shin, Se-Hoon Oh, Byung-Su Kim, and In-Jin Shon, Korean J. Met. Mater. 53 (2015) 555-562.
15. Bo-Ram Kang, Jin-kook Yoon2, Kyung-Tae Hong, and In-Jin Shon, Met. Mater. Int., Vol. 21, No. 4 (2015) 698-703.
16. In-Jin Shon, Korean J. Met. Mater. 54 (2016) 893-897.
17. C. Suryanarayana, M. Grant Norton, X-ray diffraction: a practical approach, Plenum Press, New York, 1998.
18. R.L. Coble, J. Appl. Phys. 41 (1970) 4798-4807.
19. Z. Shen, M. Johnsson, Z. Zhao, M. Nygren, J. Am. Ceram. Soc. 85 (2002) 1921-1927.
20. Yan Gu, Ping Shen, Nan-Nan Yang, Kang-Zhan Cao, Journal of Alloys and Compounds 586 (2014) 80-86.
21. Garay JE, Anselmi-Tamburini U, Munir ZA, Glade SC, Asoka- Kumar P. Appl. Phys. Lett. 85 (2004) 573-575.
22. K. Niihara, R. Morena, D.P.H. Hasselman, J. Mater. Sci. Lett. 1 (1982) 13-16.
23. Seung-Mi Kwak, Hyun-Kuk Park, and In-Jin Shon, Korean J. Met. Mater. 51 (2013) 341-348.